Chemistry SELECT

www.chemistryselect.org

A journal of ChemPubSoc Europe

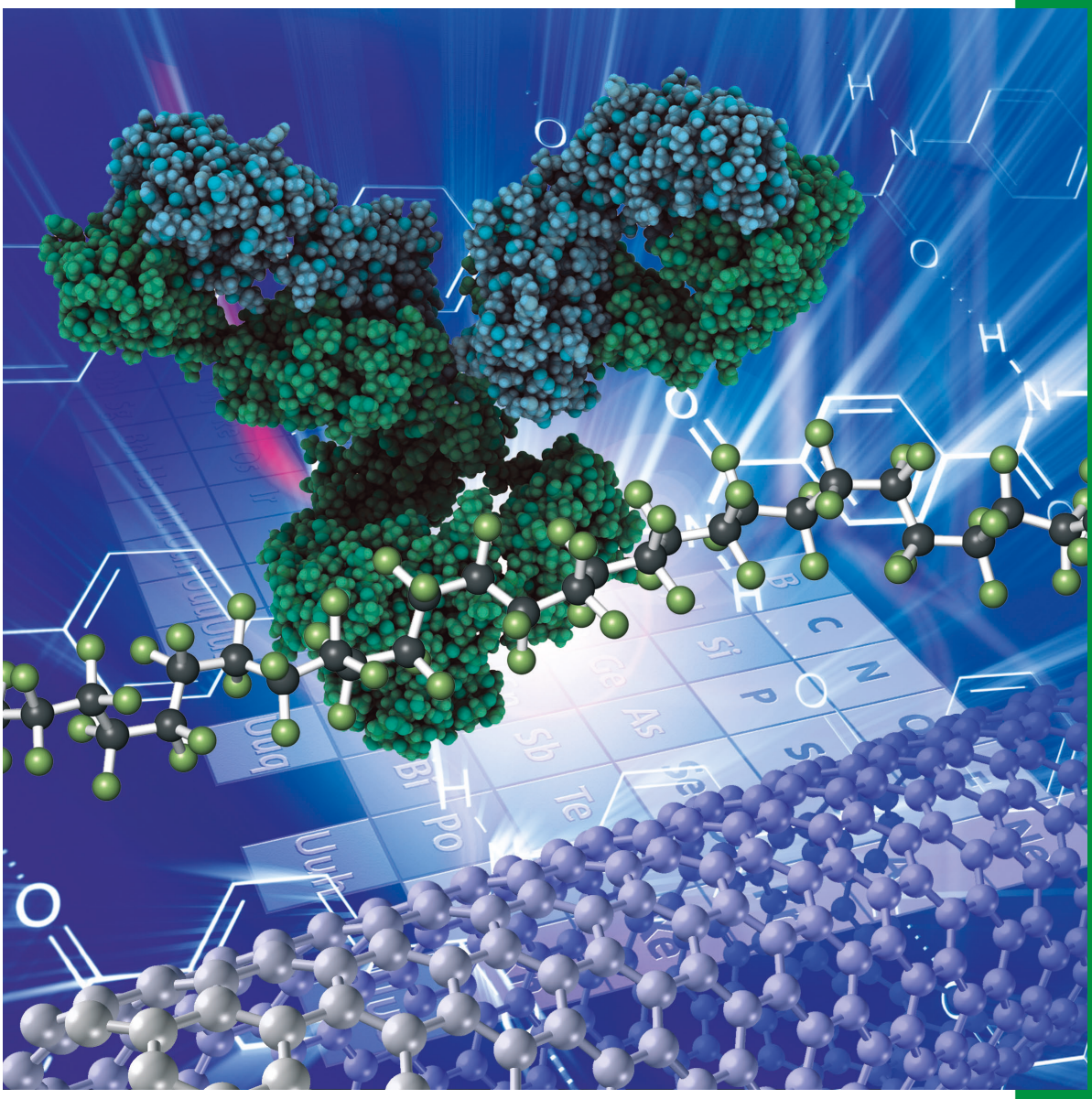

REPRINT

WILEY-VCH

ChemPubSoc Europe

DOI: 10.1002/slct.201801649

Chemistry SELECT Full Papers

Materials Science inc. Nanomaterials & Polymers

Micron-size Silicon Monoxide Asymmetric Membranes for Highly Stable Lithium Ion Battery Anode

Ji Wu,*[a] Congrui Jin,[b] Nathan Johnson,[a] Moses Kusi,[a] and Jianlin Li[c]

To meet the increasing demand for high energy density lithium ion batteries for electric vehicles and mobile electronics, it is mandatory to make revolutionary changes in electrode materials and chemistry. In this report, micron-size silicon monoxide powders are utilized to fabricate asymmetric membranes via a phase inversion method. We investigate the effects of carbonization temperature, silicon monoxide concentration and glues on membrane microstructure and electrochemical performance. It iss also observed that silicon monoxide powders in the membranes consist of silicon with multiple oxidation states. All silicon monoxide asymmetric membrane electrodes are characteristic of significantly improved cycling stability as compared to the control silicon monoxide electrode. The best cycling performance is achieved from the asymmetric membrane with lower silicon monoxide content and using carboxymethyl cellulose as the glue. 95% initial capacity can be retained after 110 cycles at 400 mA g^{-1} for the membrane with ~33 wt.% silicon monoxide. Its initial capacity loss is only 23.1% with an average coulombic efficiency of 99.82% over 110 cycles.

Introduction

Lithium Ion Batteries (LIBs) are the dominating power source for mobile electronics and all electric vehicles because of their relatively high energy and high power density, low self-discharging rate, and long cycling lifespan.[1] However, increasing energy density still remains one major challenge for LIBs for practical applications, such as extending driving range of electric vehicles, which relies on developing novel active materials with high energy density and tailored electrode engineering and architectures to minimize the inactive material content.[2] Graphite has been the conventional anodes due to its low costs and excellent cyclability, but its capacity is limited to 372 mAh g^{-1} based on LiC_6.[1b,3] In contrast, silicon (Si) as an alloying electrode material for LIB possesses an extremely high theoretical capacity (4200 mAh g^{-1} based on $Li_{22}Si_5$). Furthermore, its abundance in the earth's crust is very rich (~28 wt. %), thus bearing a great potential to replace graphite for next-generation high capacity LIB anodes. Unfortunately, Si has very poor mechanical strength and the large volume variation (~300%) during Si alloying and de-alloying with lithium can lead to fast electrode delamination and pulverization, loose contact with conductive additives and thus leading to rapid capacity fading.[1b,3–4] Furthermore the fractured silicon can cause excessive solid electrolyte interphase (SEI) growth, hence resulting in a low coulombic efficiency[5] and requiring more electrolyte.[6]

Several innovative strategies have been proposed to tackle the problems of Si anodes, most of which are associated with various kinds of nanostructures such as nanoparticles (NPs), nanowires (NWs), nanotubes (NTs), nanofibers (NFs), nanoscale thin films, mesoporous and microporous materials, and SiO_x.[3,7] Si is normally engineered into nanomaterials to overcome low diffusion coefficient of Li ions in silicon as compared to graphite (~10^{-10} vs. 10^{-6} cm^2 s^{-1})[8] and reduce Li ion diffusion length for high rate performance. Furthermore, Si NPs can better withstand the associated volume expansion in lithiation and de-lithiation process without cracking.[9] However, it is cost inhibitive to use Si NPs with current synthesis methods and low cost Si materials are needed to reduce LIB cost. One strategy would be utilizing Si micron-size powders (Si MPs) of which the cost is more than one order of magnitude lower than that of the Si NPs.[10] Moreover, Si MPs have a much higher tap density and associated larger volumetric energy density than Si NPs.[11] However, Si MPs-based anodes suffer from poor cyclability and result in cell failure in a few cycles.[11b,12] To this end, strategies have been developed to improve cyclability such as via novel binders and unique electrode architecture.[13] Recently, Cui's group synthesized novel self-healing polymers with low T_g temperatures to fill the gaps between fractured Si micron-powders, resulting in much enhanced stability (~90% capacity retention after 100 cycles).[14] Asymmetric membrane structure has been developed in our group containing micron-size Si using a highly scalable processing technology and demonstrated 32% capacity retention after 100 cycles.[15] The capacity retention can be further improved to 88% by adopting a complex triple-layer (sandwich) asymmetric membrane structure.[15]

[a] J. Wu, N. Johnson, M. Kusi
Department of Chemistry and Biochemistry, Georgia Southern University, 250 Forest Drive, Statesboro, GA 30460, USA
E-mail: jwu@georgiasouthern.edu
[b] C. Jin
Department of Mechanical Engineering, Binghamton University, 4400 Vestal Parkway East, Binghamton, NY 13902, USA
[c] J. Li
Energy & Transportation Science Division, Oak Ridge National Laboratory, Oak Ridge, TN, 37831, USA

Supporting information for this article is available on the WWW under https://doi.org/10.1002/slct.201801649

The major culprit behind the poor cyclability of Si MPS is believed to be the extremely large volume variation (300%). Thereby scientists are eagerly searching for other high capacity materials with a lower volume change to emolliate the huge mechanical stress generated during repeated cycling tests. Among these alternative materials, silicon monoxide (SiO) stands out by possessing an impressive theoretical capacity of 2400 mAh g^{-1} while its electrode volume change is less than 150%. Even though the capacity is less than 50% of Si, it is still more than four times higher than commercial graphite anode.[16] Random bonding model indicates that SiO particles consist of Si NPs (Si-rich phase) evenly distributed in SiO_2 matrix (SiO_2-rich phase).[17] Recent studies reveal that the robust SiO_2 matrix combined with the formation of lithium silicate (Li_4SiO_4) and lithium oxide (Li_2O) can ameliorate the huge volume change in silicon during lithiation and de-lithiation process,[18],[19],[20],[21][22] thus benefiting a much more stable cycling performance.[17a] The corresponding electrochemical reactions for SiO-based LIB anode are listed below:

$$4Si + 15Li^+ + 15e^- \leftrightarrow Li_{15}Si_4 \quad [1]$$

$$4SiO + 23Li^+ + 23e^- \rightarrow 4Li_2O + Li_{15}Si_4 \quad [2]$$

$$8SiO_2 + 31Li^+ + 31e^- \rightarrow 4Li_4SiO_4 + Li_{15}Si_4 \quad [3]$$

Reaction [1] is electrochemically reversible, whereas [2] and [3] are widely deemed as non-reversible.[16b,23]

Herein, low cost SiO micron powders are used to fabricate composite asymmetric membranes with excellent cyclability as compared to asymmetric membranes containing Si micron powders. As fabricated membranes are characterized using scanning electron microscopy (SEM), thermogravimetric analyzer (TGA), Energy Dispersive X-ray spectroscopy (EDS), surface area analyzer, powder X-ray diffractometer (PXRD), Raman spectroscopy and X-ray photoelectron spectroscopy (XPS). It demonstrated 99.82% coulombic efficiency and $>95\%$ capacity retention of PAN/SiO/Graphite asymmetric membrane anodes after 110 cycles at a current density of 400 mA g^{-1}.

Results and Discussion

Fabrication of asymmetric membranes containing micron-size silicon monoxide powders:

Silicon monoxide micron powder is chosen as the active material for asymmetric membrane-based LIB anode because of its low cost and mechanical robustness as compared to elemental silicon. Because the diameters of as-purchased SiO powders are very large (>10 μm) and the lithium diffusivity and electrical conductivity of SiO are quite low, these powders were ball milled (2.5 ± 2.8 μm, S2) before they were used to fabricate the membranes. The addition of carbon black is necessary to maintain the porous structure after being carbonized at high temperatures, and enhance the overall membrane conductivity. The formation mechanism of asymmetric membranes can be easily understood using a ternary phase diagram, which has been discussed explicitly in our previous studies.[24] To describe it briefly, the homogeneous phase made of solvent (N-methyl-2-pyrrolidone: NMP) and polymer (Polyacrylonitrile: PAN) is separated into two phases (polymer lean and polymer rich) after being immersed into non-solvent (deionized water), due to the mixing of solvent and non-solvent, and de-mixing of polyacrylonitrile from the solvent/non-solvent (NMP/water) mixture.[7a,25] The intrinsic 3-D porous structure and carbonaceous coating on SiO powder can efficiently accommodate large volume expansion and stabilize SEI layer, thus leading to an excellent cycling performance as confirmed by the following electrochemical tests. As compared to elemental silicon, extra protection from silica/silicate shell combining with lower volume expansion results in much improved cycling performance for SiO asymmetric membrane based LIB anode. By adding crystalline graphite (S1) and reducing the amount of SiO, the membrane electrodes become more electrically conductive with smaller volume expansion. As a result, SiO can be efficiently lithiated at a given C rate while maintaining a higher columbic efficiency since the amounts of carbon black (CB) and SiO are reduced.[26] The representative procedures used to fabricate SiO asymmetric membrane are shown in Figure 1.

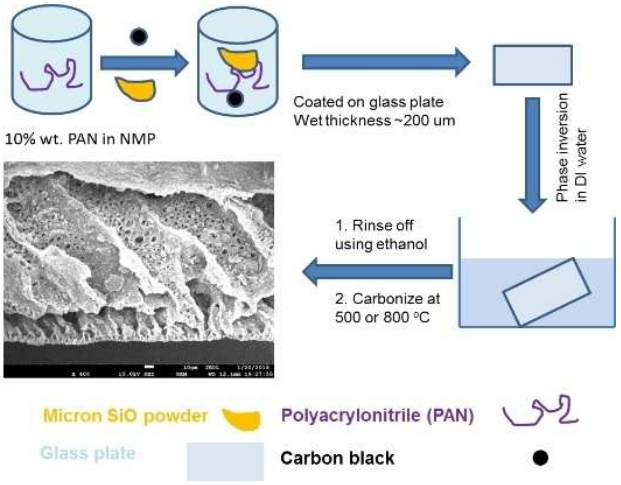

Figure 1. Schematic shows the procedures used to fabricate micron size SiO asymmetric membranes via a straightforward phase inversion method.

Material and electrode characterization:

SEM images reveal the asymmetric porous structure was maintained after the carbonization process, which consists of nanoporous skin layer and macroporous bottom layer (Figure 2). The thicknesses of PAN/SiO 500, PAN/SiO 800 and PAN/SiO/Graphite 800 were reduced to 150, 150 and 80 μm, respectively due to de-mixing and carbonization (Figure 2). PAN/SiO/Graphite 800 membrane has the largest thickness reduction because micron size graphite (S1) is not as efficient as nanoscale CB for membrane filler. However, PAN/SiO/Graphite 800 does demonstrate much enhanced cycling stability as

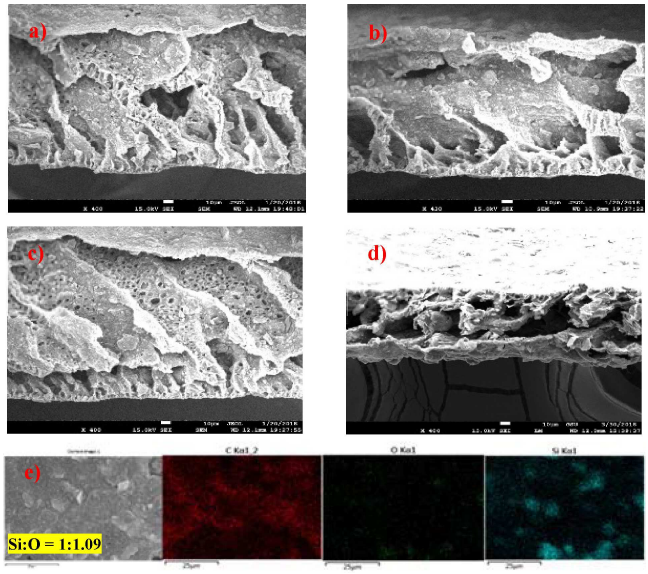

Figure 2. Scanning electron microscope images of a) PAN/SiO asymmetric membrane before carbonization; b) PAN/SiO 500 membrane; c) PAN/SiO 800 membrane; d) PAN/SiO/Graphite 800 membrane; e) EDS elemental mapping of PAN/SiO/Graphite 800 membrane.

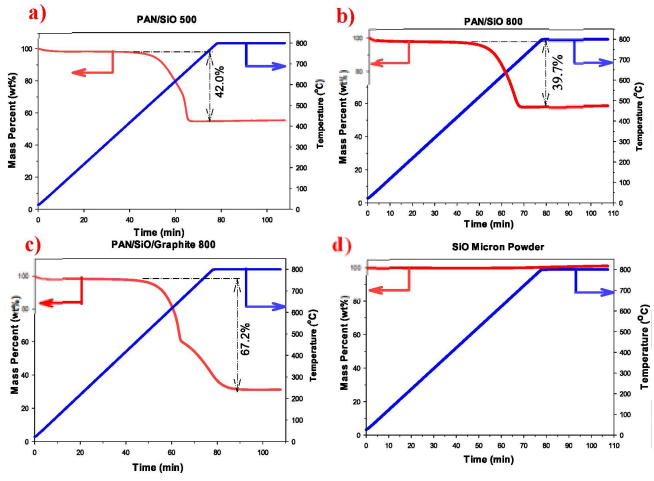

Figure 3. Thermogravimetric analysis of a) PAN/SiO 500; b) PAN/SiO 800; c) PAN/SiO/Graphite 800; d) ball milled SiO micron powders.

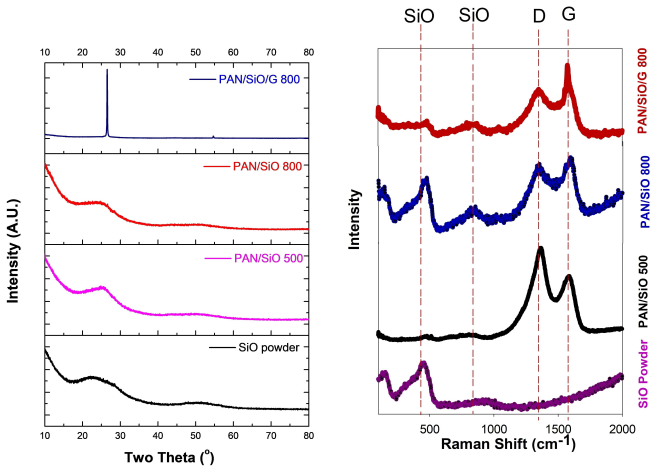

Figure 4. a) PXRD patterns and b) Raman spectra of various carbonized SiO membranes and balled milled SiO MPs

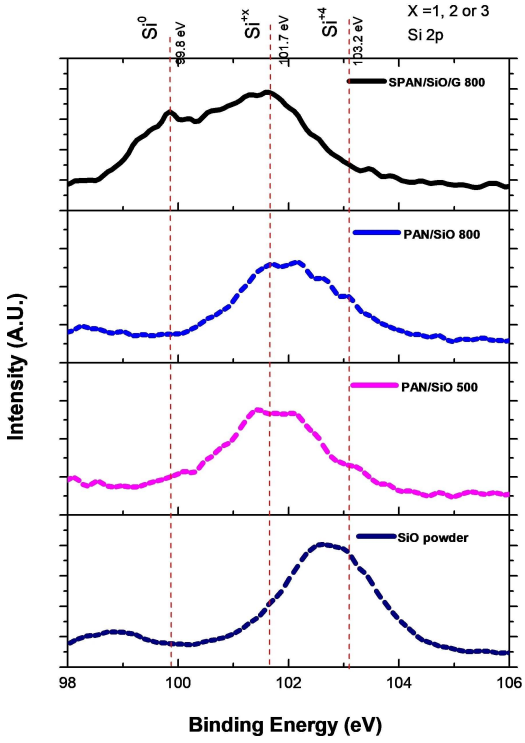

Figure 5. X-ray photoelectron spectra of various carbonized SiO membranes and ball milled SiO powders

shown in subsequent discussion compared to other membranes due to lower volume expansion and improved electrical conductivity. Corresponding EDS elemental mapping indicates that Si and O are uniformly distributed in the carbon matrix as shown Figure 2d. The atomic ratio between Si and O is measured to be 1:1.09, implying that the average oxidation state of silicon is very close to +2 as expected, which is also consistent with our XPS study that will be discussed later.

The mass percentage of active material, SiO in these asymmetric membranes was calculated from thermogravimetric analyzer data (Figure 3). The calculation is based on two facts, i.e., carbon can be oxidized into gas phase using air as the purging gas and SiO wouldn't be significantly oxidized under the same TGA conditions. Figure 3d indicates the mass of ball milled SiO powders doesn't change after being heated up to 800 °C in air (< 1 wt. %). The mass percentages of SiO in PAN/SiO 500, PAN/SiO 800 and PAN/SiO/Graphite 800 were determined to be 58 wt. %, 60 wt. % and 33 wt. %, respectively (Figure 3a-3c). It was reported that PAN tends to decompose into electrically conductive molecules with poly-pyridine structure at lower temperature like 500 °C, whereas it can be fully carbonized at 800 °C.[27] Thereby the mass percentage of

SiO in PAN/SiO 800 is slightly higher than PAN/SiO 500. The inflection point at 60 minutes in Figure 3c is due to the presence of both amorphous carbon and crystalline graphite in PAN/SiO/Graphite 800, which has been confirmed by our PXRD and Raman data shown in Figure 4. It is well known that crystalline graphite requires higher temperature to be oxidized as compared to amorphous carbon.[28]

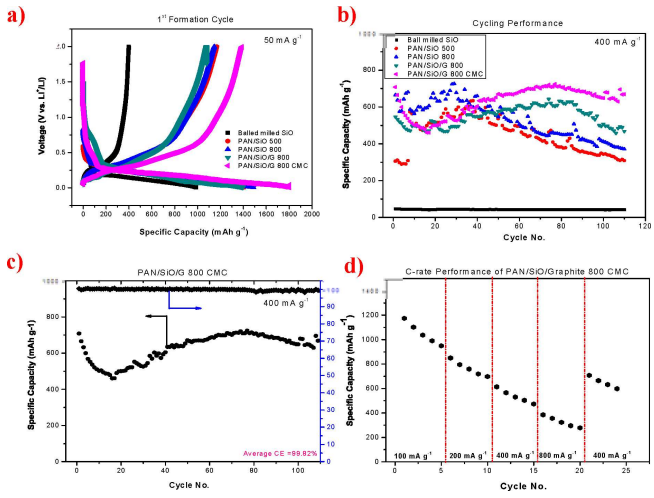

Figure 6. Electrochemical properties of SiO asymmetric membranes and balled milled SiO electrodes a) voltage profiles of the 1st formation cycle; b) cycling performance; c) cycling performance and coulombic efficiency of PAN/SiO/Graphite 800 CMC only; d) rate performance of PAN/SiO/Graphite 800 CMC only.

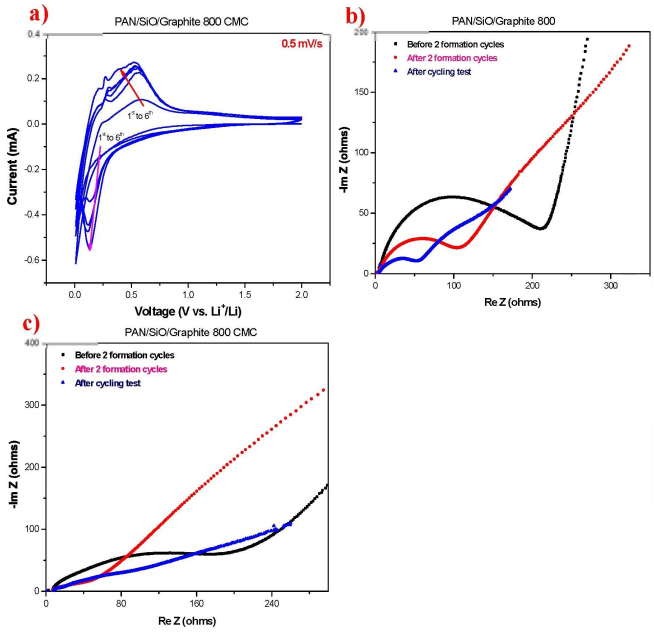

Figure 7. a) Cyclic voltammograms of PAN/SiO/Graphite 800 CMC electrode using a scanning rate of 0.5 mV/s. Nyquist plots of b) PAN/SiO/Graphite 800 electrode and c) PAN/SiO/Graphite 800 CMC electrode before and after formation cycles, and after 110 cycles

The surface areas were measured using surface area analyzer and calculated using Brunauer-Emmett-Teller (BET) equation as shown in Table 1. The specific area of balled milled

Table 1. BET surface areas of ball milled SiO powders, PAN/SiO 500, PAN/SiO 800, and PAN/SiO/Graphite 800 membranes

Sample	BET Specific Area ($m^2\ g^{-1}$)
Ball milled SiO powders	6.08 ± 0.20
PAN/SiO 500 membrane	13.21 ± 0.08
PAN/SiO 800 membrane	50.12 ± 0.91
PAN/SiO/Graphite 800 membrane	10.40 ± 0.20

SiO powders is only ~6 $m^2\ g^{-1}$. In contrast, the areas are 13.21, 50.12 and 10.40 $m^2\ g^{-1}$, respectively for PAN/SiO 500, PAN/SiO 800 and PAN/SiO/Graphite 800 membranes. The drastically increased surface areas are attributed to the highly porous structure of asymmetric membranes, including both nanopores and macropores. The area of PAN/SiO 800 is higher than PAN/SiO 500 because PAN was fully carbonized at 800 °C and thus generated more porous structure. PAN/SiO/Graphite 800 membrane has a smaller surface area due to the substitution of SiO with low surface area micron size graphite. Powder X-ray diffraction patterns of various carbonized membranes and balled milled SiO powders are shown in Figure 4a. A broad pattern around 26° can be seen from all types of membranes and SiO powders except for PAN/SiO/Graphite 800, which can be ascribed to the presence of poorly crystallized carbon and SiO materials.[7a,29] On the other hand, there is a very sharp peak at 26° from crystalline graphite (002) plane of PAN/SiO/Graphite 800 (JCPDS No. 75–1621). Broad Raman peaks cantered at 450 and 860 cm^{-1} correspond to SiO while graphite G and D peaks are located at 1570 cm^{-1} and 1351 cm^{-1}, respectively as shown in Figure 4b.[22,30] PAN/SiO/Graphite 800 possesses the highest G/D ratio because it contains crystalline graphite powders besides amorphous carbon.

Figure 5 shows the Si(2p) XPS spectra of asymmetric membranes and balled milled SiO powders. The peak with a binding energy of 99.8 eV can be assigned to elemental silicon while the oxidized silicon (IV) exhibits a weak peak at 103.2 eV. The broad peak around 101.7 eV is from partially oxidized silicon (I–III). Carbonized membranes show much weaker oxidized silicon (IV) peak, probably due to the partial reduction of silicon at elevated temperatures. The membrane containing crystalline graphite exhibits the strongest elemental silicon peak, implying graphite can reduce silicon oxides more efficiently as compared to amorphous carbon black.[5,31]

Electrochemical Analysis:

Figure 6 shows the electrochemical properties of various asymmetric membrane and ball milled SiO powders. During the first formation cycle at a current density of 50 mA g^{-1}, the lithiation and delithiation capacities of PAN/SiO/Graphite 800 electrode glued using carboxymethyl cellulose sodium salts (CMC) are 1804 and 1387 mAh g^{-1}, respectively, corresponding

to an initial capacity loss (ICL) of 23.1% (Figure 6a and Table 2). This ICL is quite similar to that of PAN/SiO/Graphite 800 and PAN/SiO 800 membranes glued using polyvinylidene difluoride (PVDF). However, the initial lithiation and de-lithiation capacities of PAN/SiO/Graphite membrane electrode glued using PVDF are only 1397 and 1078, respectively, because CMC is a better binder than PVDF for Si anodes providing stronger adhesion between CMC and SiO.[32] It is not surprising to see an ICL as high as 59.5% from ball milled SiO electrode because of electrode pulverization and delamination, as well as loose contact with conductive additives. This high ICL is close to the ones reported in literature.[33] It is interesting to find out ICL (17.1%) of PAN/SiO 500 is lower than other electrodes. The difference may be related to the highly conductive and flexible poly-pyridine structure in PAN/SiO 500. Unfortunately, it seems that PAN/SiO 500 can't stand long term cycling as evident in Figure 6.

Table 2. Initial capacity loss (ICL) of ball milled SiO powders, PAN/SiO 500, PAN/SiO 800, and PAN/SiO/Graphite 800 membrane electrodes

Sample	ICL (%)
Ball milled SiO powders	59.5
PAN/SiO 500 membrane	17.1
PAN/SiO 800 membrane	22.8
PAN/SiO/Graphite 800 membrane	22.8
PAN/SiO/Graphite 800 membrane (CMC glue)	23.1

Among all kinds of membranes, PAN/SiO/Graphite 800 glued using CMC binder demonstrates the most outstanding cyclability. 95% of its initial capacity of 708 mAh g^{-1} at 400 mA g^{-1} can be retained after 110 cycles. Assuming the capacity of carbon in the membrane electrode is 372 mAh g^{-1} (maximum possible value), the specific capacity of SiO was calculated to 1277 mAh g^{-1} after 110 cycles at 400 mA g^{-1}, which is more than 50% of the theoretical capacity of pure SiO. It is noteworthy the capacity experiences an initial loss and then increase after ~20 cycles similar to Si MPs.[15] The initial capacity loss can be ascribed to the pulverization of SiO MPs. After stable SEI layers are formed, these cracked Si particles become accessible to lithiation again, and thus regain its capacity.[15,34] It is also possible that fractured SiO nanoparticles eventually fall into the tortuous conductive carbon matrix, hence become accessible to lithiation again. in-situ SEM or TEM imaging is believed to the most critical technique to fully understand the mechanism for this interesting phenomenon. In contrast, the balled milled SiO electrodes loses almost all capacity after two formation cycles (~50 mAh g^{-1}, Figure 6b) due to serious electrode delamination and pulverization as discussed in the introduction. The significant enhanced cyclability can be attributed to the unique asymmetric porous structure combined with low content of SiO (33 wt.%), as well as the use of superior binder like CMC. When the content of SiO in asymmetric membrane is increased to ~60 wt.% (PAN/SiO 800), only 55% capacity can be maintained after 110 cycles applying the same current density. The initial capacity of PAN/SiO 800 (Figure 6b, 665 mAh g^{-1}, 61.3 wt.% SiO) is not as high as the initial capacity of PAN/SiO/Graphite 800 CMC (Figure 6c, 708 mAh g^{-1}, 33 wt.% SiO) because SiO in PAN/SiO 800 can't be fully lithiated due to its intrinsically insulating characteristic. In contrast, SiO can be more efficiently lithiated in PAN/SiO/Graphite 800 CMC because its matrix is more conductive and CMC binder has stronger adhesion force towards SiO. The cycling performance of PAN/SiO 500 that was carbonized at 500 °C with ~60 wt.% SiO powders is quite close to PAN/SiO 800. After 110 cycles, its specific capacity drops to nearly 300 mAh g^{-1} (Figure 6b). The average coulombic efficiencies of PAN/SiO/Graphite 800 and PAN/SiO/Graphite 800 CMC asymmetric membranes over 110 cycles are 99.88% and 99.82%, respectively. When the current density is increased from 100 to 800 mA g^{-1}, the capacity of PAN/SiO/Graphite 800 CMC electrode is decreased by ~66% (Figure 6d). Such a rate performance is close to our expectation, considering SiO powders are of micron size and SiO is intrinsically insulating with low lithium diffusivity. The rate performance could be further boosted by using nanoscale SiO and graphene, and special binders, although the increased cost should be of concern for practical applications. Lastly, it should be pointed out specifically such rate performance and cyclability are highly impressive compared to other reports using micron size SiO powders.[16a,35]

PAN/SiO/Graphite 800 CMC electrode was also characterized using cyclic voltammetry with a scanning rate of 0.5 mV/s as shown in Figure 7a. There is a sharp peak at lower voltage (~20 mV) during the first lithiation process, which can be attributed to both reversible and irreversible electrochemical reactions including the formation of Li_4SiO_4, Li_2O and $Li_{15}Si_4$ as discussed in the introduction.[16b] Broad delithiation peaks ranging from 0.2-0.56 V are assigned to the reversible extraction of lithium ions from $Li_{15}Si_4$ alloys.[16b] Lithiation peaks are gradually shifted to high voltages up to ~0.14 V vs. Li^+/Li as the result of the formation of stable SEI layer and thus reduced over potential. To further monitor the electrode evolution during cycling tests, electrochemical impedance spectra (EIS) were collected under delithiation state from PAN/SiO/Graphite 800 and PAN/SiO/Graphite 800 CMC electrodes shown in Figure 7b and 7c. The diameter of semicircle in the EIS Nyquist plot corresponds to charge transfer resistance (R_{ct}) at the electrode surface. As revealed in Figure 7b and 7c, R_{ct} has been significantly decreased after two formation cycles at 50 mA g^{-1} due to the formation of stable SEI layer and improved wetting of the electrode surface by electrolyte. After cycling test R_{ct} has been further reduced, implying the asymmetric porous membrane structure and SEI layer are extremely stable without significant delamination and pulverization under repeated lithiation and delithiation cycles with large electrode volume change and stress. This fact also implies SiO powders may be surrounded by carbonaceous materials, thus dramatically slowing down the formation of new SEI layer on SiO surface. To further support our claim, the cycled cell was opened to retrieve the PAN/SiO/Graphite 800 membrane electrode that has been rinsed using a large quantity of diethyl carbonate before SEM examination. Corresponding SEM images confirm

that the SEI layer is quite integral without any apparent cracks (S3). Since the electrode is composed of two dramatically different materials, i.e., graphite with higher conductivity and SiO of lower conductivity, two semicircles can be seen from both electrodes as evidenced by Figure 7.

Conclusions

Asymmetric membranes containing SiO MPs demonstrated much enhanced cycling performance as LIB anode compared to the control SiO MPs electrodes in conventional electrode structure. The outstanding cyclability is attributed to the synergic effect of 1) networking porous structure of conductive SiO asymmetric membranes which can efficiently accommodate volume expansion during lithiation and de-lithiation, 2) the robust SiO_2 matrix in SiO particle, 3) the formation of lithium oxide and lithium silicate shell layer to emolliate the stress generated during silicon alloying and 4) efficient binder like CMC that can keep the membrane electrode from being detached from the copper current collector after repeated charging/discharging. The decent rate performance is due to the existence of uniform carbonaceous coating on SiO powders after the carbonization. It's demonstrated here that the micron size SiO-based asymmetric membrane is a highly promising candidate for the next generation lithium ion battery anodes with high capacity, outstanding cyclability and decent rate performance.

Supporting Information Summary

Experimental conditions for the fabrication of SiO asymmetric membranes, and control electrodes, as well as characterizations, electrochemical analysis; S1: scanning electron microscope and transmission electron microscope images of PAN/SiO 800, PAN/SiO/Graphite 800, balled milled SiO powders and graphite powders; S2: size distribution of balled milled SiO powders; S3: scanning electron microscope images of PAN/SiO/Graphite 800 membrane electrode after 110 cycles at various magnifications.

Acknowledgements

JW deeply appreciates the funding provided by NSF-CBET award #1800619 at Georgia Southern University. JW, NJ and MK also sincerely acknowledge the financial and infrastructural supports provided by Georgia Southern University, especially 2017–2018 COUR award and 2017–2018 GSU FRC scholarly pursuit grant. Part of the research at Oak Ridge National Laboratory, managed by UT Battelle, LLC, for the U.S. Department of Energy under contract DE-AC05-00OR22725 was sponsored by the Office of Energy Efficiency and Renewable Energy Vehicle Technologies Office (VTO) Applied Battery Research (ABR) subprogram (Program Managers: Peter Faguy).

Conflict of Interest

The authors declare no conflict of interest.

Keywords: asymmetric membrane · binders · lithium ion battery anode · micron-size silicon monoxide · phase inversion

[1] aN. Nitta, F. Wu, J. T. Lee, G. Yushin, *Materials Today* **2015**, *18*, 252–264; bW. Xiao, C. Miao, X. Yan, Q. Sun, P. Mei, *Journal of Nanomaterials* **2015**, *2015*, 1–6.
[2] J. Li, Z. Du, R. E. Ruther, S. J. AN, L. A. David, K. Hays, M. Wood, N. D. Phillip, Y. Sheng, C. Mao, S. Kalnaus, C. Daniel, D. L. Wood, *JOM* **2017**, *69*, 1484–1496.
[3] D. Leblanc, P. Hovington, C. Kim, A. Guerfi, D. Bélanger, K. Zaghib, *Journal of Power Sources* **2015**, *299*, 529–536.
[4] K. Nishikawa, J. Moon, K. Kanamura, *Journal of Power Sources* **2016**, *302*, 46–52.
[5] J. Zhao, Z. Lu, H. Wang, W. Liu, H.-W. Lee, K. Yan, D. Zhuo, D. Lin, N. Liu, Y. Cui, *Journal of the American Chemical Society* **2015**, *137*, 8372–8375.
[6] S. J. An, J. Li, C. Daniel, H. M. Meyer, S. E. Trask, B. J. Polzin, D. L. Wood, *ACS Applied Materials & Interfaces* **2017**, *9*, 18799–18808.
[7] al. Byrd, H. Chen, T. Webber, J. Li, J. Wu, *RSC Advances* **2015**, *5*, 92878–92884; bT. Kim, J. Shin, T.-S. You, H. Lee, J. Kim, *Electrochimica Acta* **2015**, *164*, 227–234; cY. Wang, X. Wen, J. Chen, S. Wang, *Journal of Power Sources* **2015**, *281*, 285–292; dH. Zhang, H. Xu, *Solid State Ionics* **2014**, *263*, 23–26.
[8] R. Ruffo, S. S. Hong, C. K. Chan, R. A. Huggins, Y. Cui, *The Journal of Physical Chemistry C* **2009**, *113*, 11390–11398.
[9] Z. Chen, C. Wang, J. Lopez, Z. Lu, Y. Cui, Z. Bao, *Advanced Energy Materials* **2015**, *5,* 1401826.
[10] S. P. V. Nadimpalli, V. A. Sethuraman, S. Dalavi, B. Lucht, M. J. Chon, V. B. Shenoy, P. R. Guduru, *Journal of Power Sources* **2012**, *215*, 145–151.
[11] a) D. Lin, Z. Lu, P.-C. Hsu, H. R. Lee, N. Liu, J. Zhao, H. Wang, C. Liu, Y. Cui, *Energy & Environmental Science* **2015**, *8*, 2371–2376; b) C. Wang, H. Wu, Z. Chen, M. T. McDowell, Y. Cui, Z. Bao, *Nature Chemistry* **2013**, *5*, 1042–1048.
[12] M. Wu, J. E. C. Sabisch, X. Song, A. M. Minor, V. S. Battaglia, G. Liu, *Nano Letters* **2013**, *13*, 5397–5402.
[13] K. A. Hays, R. E. Ruther, A. J. Kukay, P. Cao, T. Saito, D. L. Wood, J. Li, *Journal of Power Sources* **2018**, *384*, 136–144.
[14] C. Wang, H. Wu, Z. Chen, M. T. McDowell, Y. Cui, Z. Bao, *Nat Chem* **2013**, *5*, 1042–1048.
[15] I. Byrd, J. Wu, *Electrochimica Acta* **2016**, *213*, 46–54.
[16] a) S. Goriparti, E. Miele, F. De Angelis, E. Di Fabrizio, R. Proietti Zaccaria, C. Capiglia, *Journal of Power Sources* **2014**, *257*, 421–443; b) J. K. Lee, W. Y. Yoon, B. K. Kim, *Journal of The Electrochemical Society* **2014**, *161*, A927-A933.
[17] a) Y.-H. Liu, M. Okano, T. Mukai, K. Inoue, M. Yanagida, T. Sakai, *Journal of Power Sources* **2016**, *304*, 9–14; b) K. Xu, *Chemical Reviews* **2014**, *114*, 11503–11618.
[18] R. Teki, M. K. Datta, R. Krishnan, T. C. Parker, T.-M. Lu, P. N. Kumta, N. Koratkar, *Small* **2009**, *5*, 2236–2242.
[19] H. Li, X. Huang, L. Chen, Z. Wu, Y. Liang, *Electrochemical and Solid-State Letters* **1999**, *2*, 547–549.
[20] W.-J. Zhang, *Journal of Power Sources* **2011**, *196*, 877–885.
[21] G. K. Simon, T. Goswami, *Metallurgical and Materials Transactions A* **2011**, *42*, 231–238.
[22] J. Woo, S.-H. Baek, J.-S. Park, Y.-M. Jeong, J. H. Kim, *Journal of Power Sources* **2015**, *299*, 25–31.
[23] H. J. Kim, S. Choi, S. J. Lee, M. W. Seo, J. G. Lee, E. Deniz, Y. J. Lee, E. K. Kim, J. W. Choi, *Nano Letters* **2016**, *16*, 282–288.
[24] J. Wu, H. Chen, I. Byrd, S. Lovelace, C. Jin, *ACS Applied Materials & Interfaces* **2016**, *8*, 13946–13956.
[25] L. F. Greenlee, D. F. Lawler, B. D. Freeman, B. Marrot, P. Moulin, *Water Research* **2009**, *43*, 2317–2348.
[26] J. Wutthiprom, N. Phattharasupakun, M. Sawangphruk, *ACS Omega* **2017**, *2*, 3730–3738.
[27] N. Grassie, R. McGuchan, *European Polymer Journal* **1970**, *6*, 1277–1291.
[28] Q. Wu, T. Tran, W. Lu, J. Wu, *Journal of Power Sources* **2014**, *258*, 39–45.

[29] a) M. Todica, T. Stefan, S. Simon, I. Balasz, L. Daraban, *Turkish Journal of Physics* **2014**, *38*, 261–267; b) A. Magasinski, P. Dixon, B. Hertzberg, A. Kvit, J. Ayala, G. Yushin, *Nat Mater* **2010**, *9*, 461–461.
[30] T. P. Nguyen, S. Lefrant, *Solid State Communications* **1986**, *57*, 235–236.
[31] J. W. He, X. Xu, J. S. Corneille, D. W. Goodman, *Surface Science* **1992**, *279*, 119–126.
[32] a) J. Li, R. B. Lewis, J. R. Dahn, *Electrochemical and Solid-State Letters* **2007**, *10*, A17-A20; b) P.-F. Cao, M. Naguib, Z. Du, E. Stacy, B. Li, T. Hong, K. Xing, D. N. Voylov, J. Li, D. L. Wood, A. P. Sokolov, J. Nanda, T. Saito, *ACS Applied Materials & Interfaces* **2018**, *10*, 3470–3478.
[33] T. Chen, J. Wu, Q. Zhang, X. Su, *Journal of Power Sources* **2017**, *363*, 126–144.
[34] C. Wang, H. Wu, Z. Chen, M. T. McDowell, Y. Cui, Z. Bao, *Nature Chemistry* **2013**, *5*, 1042.
[35] a) T. Huang, Y. Yang, K. Pu, J. Zhang, M. Gao, H. Pan, Y. Liu, *RSC Advances* **2017**, *7*, 2273–2280; b) C.-H. Doh, C.-W. Park, H.-M. Shin, D.-H. Kim, Y.-D. Chung, S.-I. Moon, B.-S. Jin, H.-S. Kim, A. Veluchamy, *Journal of Power Sources* **2008**, *179*, 367–370.

Submitted: May 30, 2018
Accepted: July 28, 2018